Check for updates

Hydrated FePO₄ nanoparticles supported on P-doped RGO show enhanced ORR activity compared to their dehydrated form in an alkaline medium†

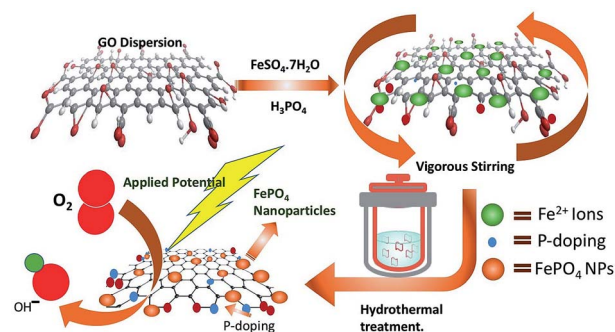Zubair Ahmed,[a] Ritu Rai,[a] Rajinder Kumar,[a] Takahiro Maruyama[b] and Vivek Bagchi (ORCID) *[a]

One-step hydrothermal growth of FePO₄ nanoparticles (15–25 nm) uniformly decorated on the P-doped reduced graphene oxide (PRGO) was studied for oxygen reduction reaction (ORR) activity. The role of lattice water in the enhancement of catalytic activity in the hydrated FePO₄·2H₂O with respect to its dehydrated form in the alkaline medium was contested. The hydrodynamic LSV at 1600 rpm in alkaline medium (0.1 M KOH electrolyte) indicates an increase in the cathodic current density of the PRGO supported FePO₄·2H₂O catalyst, which reaches as high as 5.8 mA cm⁻², close to the best known commercially available Pt/C catalyst. The stability in terms of retention of activity after 22 000 s with the hydrated form was found to be 90.7% which is 26.7% higher than that of the dehydrated form.

Introduction

Overconsumption of fossil fuels and the various environmental issues have greatly motivated the scientific community towards the advancement of sustainable technologies specifically, fuel cells,[1,2] metal–air batteries[3–5] and solar cells.[6–8] The advances in the field of fuel cell technology are mainly affected by the sluggish kinetics of the oxygen reduction reaction; therefore the development of a highly efficient catalyst for ORR is highly desirable. So far platinum and platinum group metals have emerged to be highly proficient catalysts for ORR. However, high cost, surface corrosion as well as methanol poisoning are some of the major flaws which deteriorate their practical applicability.[9] Several attempts have been made to judiciously design non-nobel metal catalysts with performance similar to or better than Pt-based electrocatalysts, which include chalcogenides,[10] transition metal oxides,[11] carbides,[12] phosphides[13] and nitrides,[14] as well as metal-free carbon-based materials.[15] Owing to the high catalytic efficiency and stability, transition metal phosphates have gathered tremendous attention in recent years as they have the capability of influencing both the water oxidation as well as the electrocatalytic oxygen reduction. Several groups have found that the catalyst composed of Pt supported metal phosphates[16,17] have shown superior ORR activity as compared

to commercial Pt/C. Furthermore, metal-free, doped (B, S, N, P *etc*) carbonaceous materials have also shown their potential in the area of ORR catalysis[18–22] as the introduction of heteroatoms into the graphite lattice not only enhances the conductivity but also provides strong support for holding the active sites.[23–25] However, research efforts towards exploring the efficacy of metal phosphates as ORR catalysts are still limited.[26] Thus the design and fabrication of highly efficient transition metal phosphates through a simple yet cost-effective methodology would provide a vision for a new class of catalytic materials for ORR. Herein we have used a one-pot hydrothermal method (as shown in Scheme 1) to synthesize FePO₄ nanoparticles systematically grown on P-doped RGO and studied the ORR activities in the alkaline medium. To the best of our knowledge, the crucial role of lattice water of FePO₄

[a]Institute of Nano Science and Technology, Phase-10, Sector-64, Mohali, Punjab 160062, India. E-mail: vivekbagchi@gmail.com; bagchiv@inst.ac.in

[b]Department of Applied Chemistry, Meijo University, 1-501 Shiogamaguchi, Tempaku, Nagoya 468-8502, Japan

Scheme 1 Showing the overall synthesis of the hybrid-nanocomposite using hydrothermal growth of FePO₄ nanoparticles (15 to 25 nm) uniformly decorated on the P-doped RGO as an electrocatalyst for oxygen reduction reaction (ORR).

in enhancing the catalytic activity, particularly for oxygen reduction electrocatalysis has never been explored.

Experimental

Graphene nanoplatelets (<25 μm) were purchased from (TCI). Orthophosphoric acid (H_3PO_4), sulphuric acid (H_2SO_4) and potassium permanganate ($KMnO_4$) were purchased from Merck. Graphene oxide was synthesized by an improved method[27] using graphene nanoplatelets. The catalyst was synthesized by a one-step hydrothermal process. In brief, 0.2 mM (55 mg) of $FeSO_4\cdot7H_2O$ was added into the uniform dispersion of graphene oxide (1 mg ml^{-1}) in distilled water with vigorous stirring. Orthophosphoric (1 ml of 3 M) acid was added dropwise with continuous stirring for 30 min. The reaction mixture was transferred into a stainless steel autoclave with Teflon vessel inside and kept at 180 °C for 12 h. The obtained product (FePH@PRGO) was washed with deionised water and further dried by heating it at 50 °C for 4 hours. The dehydrated product (FePD@PRGO) was obtained by annealing FePH@PRGO in argon at 300 °C for 30 minutes. A batch of P-doped RGO was synthesized by the same method for a comparative study.

Characterization

The structural and morphological characterization were done using Eco D8 advance from Bruker, Cu Kα radiation with $\lambda = 1.54$ Å; Scanning Electron Microscope (JEOL JSM-IT300) was used for the morphological studies. Transmission electron microscopy using JEM-2100 TEM has been used at 200 kV to obtain the high-resolution TEM images. X-ray photoelectron spectroscopy (XPS, EscaLab: 220-IXL) was used to analyse the composition of the electrocatalyst by means of Mg-Kα non-monochromated X-ray beam having photon energy of 1253.6 eV. Surface area and pore size distribution were determined from N_2 adsorption and desorption using (Autosorb-iQ) Quantachrome Instrument; thermogravimetric analysis was done using STA-8000 (Perkin Elmer); FTIR spectra were recorded on Carry 660 FTIR spectrometer.

Electrochemical measurements

Electrochemical measurements were performed on an multi-channel electrochemical workstation (Autolab PGSTAT 204M) equipped with electrode bipotentiostat system. Carbon electrode, Ag/AgCl (3 M KCl solution) and Rotating Ring Disk Electrode (RRDE) having a diameter of 5 mm were used as a counter, reference and working electrode respectively. The working electrode was coated with 10 μl of the catalyst ink which was prepared by dispersing 2 mg catalyst in 495 μl DMF and 5 μl of 5% Nafion. The catalyst coated electrode surface was dried in vacuum for overnight to get a uniform layer of material on the electrode surface. Cyclic voltammetry (CV) and linear sweep voltammetry (LSV) were performed in O_2 saturated 0.1 M KOH by purging electrolyte with O_2 30 min prior to electrochemical measurements. Several CV scanning was done with a scan rate of 50 mV $^{-1}$ in the potential window of 0 to −1.0 V. LSV measurements were carried out in a potential window of 0.1

to −1 V with a scan rate of 10 mV s^{-1} on RRDE with rotating speed varying from 400 to 3000 rpm.

Recently it has been revealed that the extensively used Koutechy–Levich (KL) method is not appropriate to evaluate "n" for the ORR studies.[28] Hence, the rotating disk and ring-disk electrodes were analysed using convection methods for the calculation of the electron transfer number "n" for the oxygen reduction reaction (ORR) on the corresponding catalyst and the peroxide percentage was calculated using ring and disc current is given by eqn (1) and (2) respectively.

$$n = 4 \times \frac{I_d}{I_d + I_r/N} \tag{1}$$

$$HO_2^-\% = 200 \times \frac{I_r/N}{I_d + I_r/N} \tag{2}$$

where I_d and I_r represent disk and ring current respectively. N is defined as the current collection efficiency of Pt ring which was found to be 0.25 long term catalytic stability was examined by chronoamperometric measurements performed at −0.6 V with a rotation of 1600 rpm.

Results and discussion

The $FePO_4$ nanoparticles supported on P-doped RGO was synthesized both in hydrated (FePH@PRGO) and dehydrated form (FePD@PRGO) using the one-pot hydrothermal method. Here orthophosphoric acid (H_3PO_4) plays a bifunctional role as it facilitates the formation of phosphate nanoparticles and the incorporation of P atom in the graphitic lattice which in turn enhances the overall performance of the catalyst. Since the product obtained does not require any further purification thus holding the integrity of the process.

The oxygen reduction activity of the catalysts was evaluated using CV studies carried out in O_2 saturated 0.1 M KOH solutions for both FePD@PRGO and FePH@PRGO along with Pt/C shown in Fig. 1(A). The presence of prominent
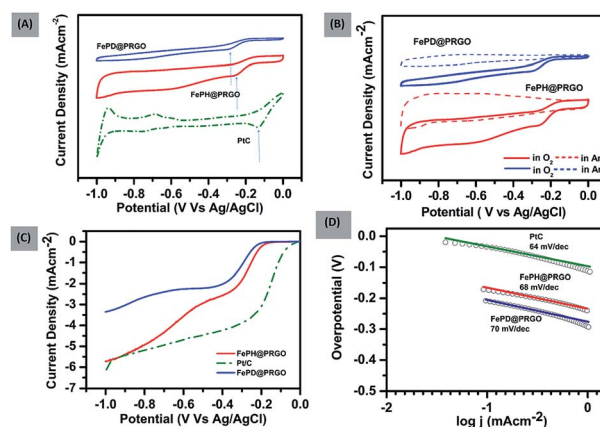

Fig. 1 (A) CV curves of FePH@PRGO, FePD@PRGO and Pt/C (B) CV curves of FePH@PRGO and FePD@PRGO in Ar and O_2 saturated 0.1 M KOH electrolyte. (C) LSV curves of FePD@PRGO, FePH@PRGO and Pt/C at 1600 rpm (D) Tafel slope of FePH@PRGO, FePD@PRGO and Pt/C.

cathodic reduction peak in O_2 saturated electrolyte as well as the absence of the same for both the catalyst in Ar saturated electrolyte reflects their activity for ORR Fig. 1(B). The cathodic reduction peak of O_2 for FePH@PRGO as well as FePD@PRGO appears approximately at −0.24 V and −0.28 V respectively. Also, the FePH@PRGO catalyst outperforms by showing relatively higher current density (Fig. 1(A)). This observation directly indicates the crucial role of lattice water in facilitating ion transport. The superior catalytic activity of FePH@PRGO was also reflected in LSV measurements where the limiting current density reaches to −5.8 mA cm^{-2} with onset potential (−0.140 V) for FePH@PRGO which is very much close to Pt/C whereas, it reaches up to −3.4 mA cm^{-2} for FePD@PRGO (Fig. 1(C)). Furthermore, FePH@PRGO catalyst shows a smaller value of Tafel slope (68 mV dec^{-1}) also reflects its efficacy for ORR catalysis (Fig. 1(D)).

To further explore the kinetics and mechanistic aspects of ORR catalysis, LSV measurements of FePH@PRGO were performed at different rotations using RRDE, ranging from 400 to 3000 rpm shown in Fig. 2(A). Similar measurements were also done for FePD@PRGO and PRGO as shown in (ESI S1.1A and 2A†).

It was observed that limiting current density rises with an increase in rotational speed owing to the shortening of the diffusion distance in oxygen saturated electrolyte at high speed.[29] The K–L (Koutechy–Levich) plots corresponding to the above mentioned LSV measurements are shown in Fig. 2(B) and (ESI S1.1B and 2B†). The occurrence of first-order kinetics for the reduction of dissolved oxygen is reflected by the K–L curves which are linear in nature at every potential.

The number of electrons transferred (n) was calculated with the ring and disk plot Fig. 2(C) obtained at 1600 rpm and the value of n at different potentials (−0.40 to −0.95 V) was calculated to be in the range from ∼3.0–3.8. The corresponding ring and disk curve, suggests that the reaction is proceeding dominantly through a four-electron pathway for O_2

reduction Fig. 2(D). The major challenges associated with the ORR electrocatalysts is methanol crossover effect which decreases the efficiency of fuel cell significantly and long term stability of the catalysts.[30] The methanol poisoning of the catalyst was checked through cyclic voltammetry where 3 molar methanol is added to the electrolyte, FePH@PRGO shows high stability towards methanol oxidation with no significant change in CV curve whereas Pt/C, on the other hand, shows methanol oxidation and depressed the O_2 reduction as shown in Fig. 3(A) and (B) respectively. The long term stability of electrocatalyst was further checked through (i–t) chronoamperometry measurements after 22 000 s at −0.6 V with 1600 rpm under continuous oxygen flow. The catalyst was found to be quiet stable even after 22 000 s with a slight decline of performance (−9.3%) shown in Fig. 3(A) inset. The dehydrated form was found to be less stable and is shown in ESI S1.1C.† All the values related to ORR activities were tabulated in ESI S2.†

The composition of the catalysts, FePH@PRGO and FePD@PRGO were analysed using both PXRD and XPS. Typically, the peaks in the PXRD pattern (Fig. 4(A)) of FePH@PRGO can be indexed into a mixture of the monoclinic phase of $FePO_4 \cdot 2H_2O$ with space group $P21/n$ and lattice parameters, $a = 0.530$ nm, $b = 0.975$ nm $c = 0.867$ nm (ref. 31) and of the tetragonal $Fe_{1.37}(PO_4)(OH)$ phase with lattice parameter $a = b = 0.519$ nm and $c = 1.299$ nm and space group $I41$. High cyclic durability of the catalyst might be due to the lattice water present in FePH@PRGO catalyst. Annealing results in the formation of the catalyst FePD@PRGO with the later phase only.[32]

In the XPS spectra Fig. 4(B) two prominent peaks at 711.08 eV and 725.08 eV, corresponding to Fe $2p_{3/2}$ and Fe $2p_{1/2}$, are present. The Fe $2p_{3/2}$ peak is comprising of two peaks at 710.2 eV (Fe^{2+}) and 711.6 eV (Fe^{3+}) and the Fe $2p_{1/2}$ can also be split into two peaks at 724 eV (Fe^{2+}) and 725.8 eV (Fe^{3+}) respectively. The deconvoluted P 2p spectrum (Fig. 4(C)) revealed two peaks positioned at 133.1 and 134.1 eV, which may be attributed to P–C and P–O bonding. In Fig. 4(D), the C 1s spectrum, the major peak at 284.5 eV was due to sp^2 C–C bonding, whereas the peaks at 286.1 eV and 288.5 eV are resulting from C–O and O–C=O bonding. XPS survey spectra of FePH@PRGO was shown in ESI S3.† Thus both XPS and XRD
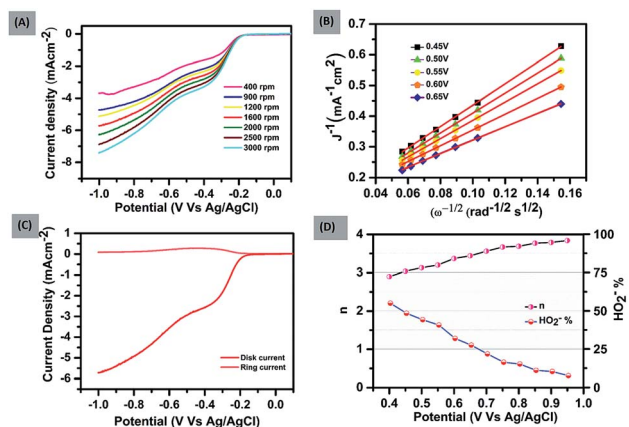

Fig. 2 (A) LSV curves of FePH@PRGO at various rotation speeds. (B) K–L plot of FePH@PRGO at various potentials. (C) RRDE curves of FePH@PRGO at a rate of 1600 rotations per minute. (D) The right vertical axis shows the HO_2^- yields where as the left axis reveals the corresponding electron-transfer number (n) of FePH@PRGO.
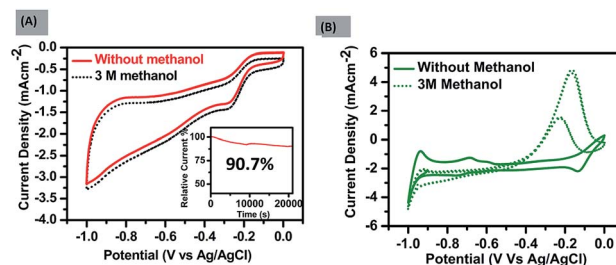

Fig. 3 Methanol crossover tests were performed with 3 M methanol on (A) the catalyst FePH@PRGO and on (B) Pt/C. The current vs. time (i–t) plot shown in inset (A), reveals a long term stability of FePH@PRGO retaining 90.7% activity after 22 000 s.
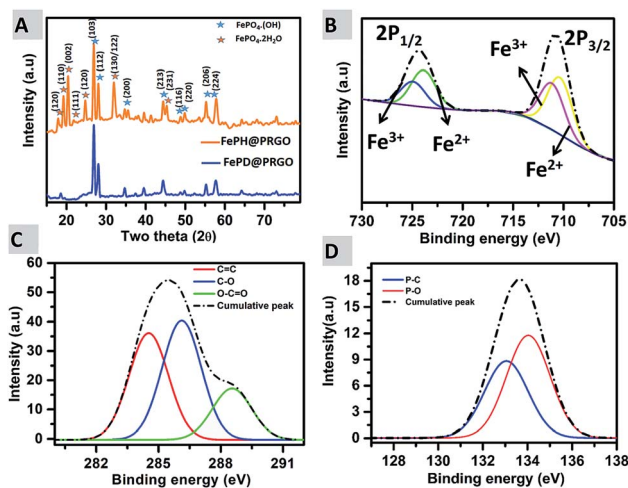
Fig. 4 (A) PXRD showing the hydrated and dehydrated forms; FePH@PRGO & FePD@PRGO (B) high-resolution X-ray photoelectron spectra of Fe 2p, (C) showing the plot for C 1s, and (D) P 2p.

successfully reveal the formation of $FePO_4$ nanoparticles supported on P doped RGO.

Further, the qualitative, as well as quantitative analysis of lattice water, was done using FTIR and TGA. The presence of lattice water was qualitatively depicted from Fourier transmission spectroscopy where the strong stretching vibrations of H_2O group at 3400 cm^{-1} are present in the spectra of FePH@PRGO whereas the peak at 3400 cm^{-1} reduced significantly in the dehydrated form as shown in Fig. 5(A).

A quantitative analysis of the amount of lattice water present in the FePH@PRGO catalyst was done using thermogravimetric analysis. TGA analysis was performed under aerobic environment in the temperature range of 50–700 °C. Fig. 5(B), shows a clear and sharp weight loss of approximately 19% depicted from the TGA curve may be correlated to the dehydration of $FePO_4 \cdot 2H_2O$. The FePD@PRGO composite was obtained by annealing FePH@PRGO which results in partial reduction of Fe^{3+} to Fe^{2+} ions in the presence of carbon from PRGO.[33] In oxidizing conditions the weight gain observed in FePD@PRGO at low temperature is possibly due to the partial oxidation of Fe^{2+} ions, resulting small weight gain (~4.4%). The small weight loss during the temperature range of 300 to 500 °C is due

to the slow decomposition of residual oxygen containing functional groups present on phosphorous doped reduced graphene oxide.[34,35] The weight loss at higher temperature ranging between temperature 500–600 °C is majorly associated with rapid burning of the ring carbon in PRGO.[36] However the higher amount of weight loss in FePD@PRGO is possibly due to the removal of OH bonds present in $FePO_4 \cdot OH$ (FePD@PRGO) which takes place in this temperature range.[37] The observations obtained from N_2 adsorption and desorption isotherm were also in line with the previous elucidations. The isotherm of both FePH@PRGO and FePD@PRGO are of "type IV" hysteresis curve shown in ESI Fig. S4A and B.† The surface area of FePD@PRGO comes out to be 185.20 m^2 g^{-1} with an average pore size of 1.9 nm, whereas the surface area of FePH@PRGO is 55 m^2 g^{-1} such a noticeable difference in the surface area can be explained due to the saturation of pores with the lattice water. In spite of high surface area, FePD@PRGO catalyst still struggles to exhibit good catalytic activity. Thus, it can undoubtedly be inferred that it is the lattice water which is playing a crucial role in enhancing the catalytic activity.

The structure and morphology of the FePH@PRGO catalyst were analysed using TEM shown in Fig. 6. Uniform nanoparticles of size ranging from 15–25 mm were distributed on the P doped graphite lattice. The inter-planar distance of 0.36 nm (Fig. 6(B)) was obtained which is consistent with the corresponding inter-planar distance of (120) plane in the monoclinic phase of $FePO_4 \cdot 2H_2O$. The morphology of FePD@PRGO is shown in ESI S5.† The phosphorous doping in RGO was verified both qualitatively and quantitatively by elemental mapping and EDAX plot. The binding energy plot shows that P doping has taken place in RGO with an atomic percentage of 1.28% as shown in ESI S6.† The electrocatalyst after the stability measurement was recovered from the electrode surface for morphological studies. The TEM/HRTEM analysis was carried
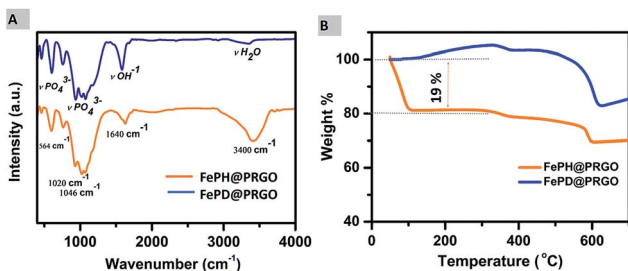

Fig. 5 (A) FTIR spectra of FePH@PRGO and FePD@PRGO. (B) Thermogravimetric analysis curves of FePH@PRGO and FePD@PRGO under air atmosphere.
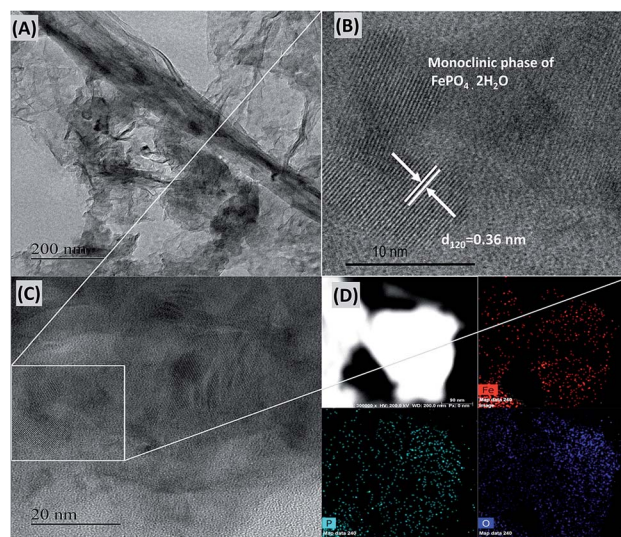

Fig. 6 (A) TEM image of FePH@PRGO (B) and (C) are the high resolution TEM images, where (B) is the zoomed version of (C) showing the fringe width of the nano crystal. (D) STEM and corresponding elemental mapping of FePH@PRGO.

out to ensure the structural stability of the FePH@PRGO shown in ESI S7.†

Conclusions

Thus we conclude that non-noble metal based nanocomposite of $FePO_4$ nanoparticles supported on P-doped RGO shows enhanced ORR activity compared to its dehydrated form. The study reveals that the lattice water in hydrated $FePO_4$ catalyst plays a crucial role in enhancing the electrocatalytic oxygen reduction and provides extra stability to the catalyst in alkaline medium, which is relatively better than its dehydrated form obtained after annealing catalyst. This work highlights the role of water molecules present in the $FePO_4$ crystal lattice in electrocatalytic ORR and unlocks a new horizon showing the possibilities of various low cost metal phosphates as catalyst in the fuel cell applications.

Conflicts of interest

There are no conflicts to declare.

Acknowledgements

Notes and references

1 W. Zhang, W. Lai and R. Cao, *Chem. Rev.*, 2017, **117**, 3717–3797.

2 D. Banham and S. Ye, *ACS Energy Lett.*, 2017, **2**, 629–638.

3 Z.-Q. Liu, H. Cheng, N. Li, T. Y. Ma and Y.-Z. Su, *Adv. Mater.*, 2016, **28**, 3777–3784.

4 J. Liu, C. Guan, C. Zhou, Z. Fan, Q. Ke, G. Zhang, C. Liu and J. Wang, *Adv. Mater.*, 2016, **28**, 8732–8739.

5 S. S. Shinde, C. H. Lee, J.-Y. Yu, D.-H. Kim, S. U. Lee and J.-H. Lee, *ACS Nano*, 2018, **12**, 596–608.

6 D. Zhao, C. Chen, C. Wang, M. M. Junda, Z. Song, C. R. Grice, Y. Yu, C. Li, B. Subedi, N. J. Podraza, X. Zhao, G. Fang, R.-G. Xiong, K. Zhu and Y. Yan, *Nat. Energy*, 2018, **3**, 1093–1100.

7 E. Kabir, P. Kumar, S. Kumar, A. A. Adelodun and K.-H. Kim, *Renewable Sustainable Energy Rev.*, 2018, **82**, 894–900.

8 J. Hou, O. Inganäs, R. H. Friend and F. Gao, *Nat. Mater.*, 2018, **17**, 119.

9 H. Tang, J. Luo, X. L. Tian, Y. Dong, J. Li, M. Liu, L. Liu, H. Song and S. Liao, *ACS Appl. Mater. Interfaces*, 2018, **10**, 11604–11612.

10 Y. Tang, T. Chen, W. Guo, S. Chen, Y. Li, J. Song, L. Chang, S. Mu, Y. Zhao and F. Gao, *J. Power Sources*, 2017, **362**, 1–9.

11 Y.-Q. Lyu, C. Chen, Y. Gao, M. Saccoccio and F. Ciucci, *J. Mater. Chem. A*, 2016, **4**, 19147–19153.

12 T. Huang, S. Mao, H. Pu, Z. Wen, X. Huang, S. Ci and J. Chen, *J. Mater. Chem. A*, 2013, **1**, 13404–13410.

13 C. Han, X. Bo, Y. Zhang, M. Li, A. Wang and L. Guo, *Chem. Commun.*, 2015, **51**, 15015–15018.

14 Y. Dong and J. Li, *Chem. Commun.*, 2015, **51**, 572–575.

15 Y. Dong, Y. Deng, J. Zeng, H. Song and S. Liao, *J. Mater. Chem. A*, 2017, **5**, 5829–5837.

16 C. Kim, B. Lee, Y. Park, B. Park, J. Lee and H. Kim, *Appl. Phys. Lett.*, 2007, **91**, 113101.

17 P. J. Bouwman, W. Dmowski, J. Stanley, G. B. Cotten and K. E. Swider-Lyons, *J. Electrochem. Soc.*, 2004, **151**, A1989–A1998.

18 L. Yang, S. Jiang, Y. Zhao, L. Zhu, S. Chen, X. Wang, Q. Wu, J. Ma, Y. Ma and Z. Hu, *Angew. Chem., Int. Ed.*, 2011, **50**, 7132–7135.

19 Z. Yang, Z. Yao, G. Li, G. Fang, H. Nie, Z. Liu, X. Zhou, X. A. Chen and S. Huang, *ACS Nano*, 2011, **6**, 205–211.

20 K. Gong, F. Du, Z. Xia, M. Durstock and L. Dai, *science*, 2009, **323**, 760–764.

21 J. Zhu, M. Xiao, P. Song, J. Fu, Z. Jin, L. Ma, J. Ge, C. Liu, Z. Chen and W. Xing, *Nano Energy*, 2018, **49**, 23–30.

22 I. Y. Jeon, S. Zhang, L. Zhang, H. J. Choi, J. M. Seo, Z. Xia, L. Dai and J. B. Baek, *Adv. Mater.*, 2013, **25**, 6138–6145.

23 H. Cui, Z. Zhou and D. Jia, *Mater. Horiz.*, 2017, **4**, 7–19.

24 C. Tang and Q. Zhang, *Adv. Mater.*, 2017, **29**, 1604103.

25 J. Jin, F. Pan, L. Jiang, X. Fu, A. Liang, Z. Wei, J. Zhang and G. Sun, *ACS Nano*, 2014, **8**, 3313–3321.

26 M. Pramanik, C. Li, Y. V. Kaneti and Y. Yamauchi, *Chem. Commun.*, 2017, **53**, 5721–5724.

27 D. C. Marcano, D. V. Kosynkin, J. M. Berlin, A. Sinitskii, Z. Sun, A. Slesarev, L. B. Alemany, W. Lu and J. M. Tour, *ACS Nano*, 2010, **4**, 4806–4814.

28 R. Zhou, Y. Zheng, M. Jaroniec and S.-Z. Qiao, *ACS Catal.*, 2016, **6**, 4720–4728.

29 W. Y. Xing, G. Yin, J. Zhang, *Rotating Electrode Methods and Oxygen Reduction Electrocatalysts*, Elsevier, Amsterdam, 2014.

30 Y. Shao, G. Yin and Y. Gao, *J. Power Sources*, 2007, **171**, 558–566.

31 K. Zaghib and C. Julien, *J. Power Sources*, 2005, **142**, 279–284.

32 Y. Song, P. Y. Zavalij, N. A. Chernova and M. S. Whittingham, *Chem. Mater.*, 2005, **17**, 1139–1147.

33 Y. Wang, M.-Q. Wang, L.-L. Lei, Z.-Y. Chen, Y.-S. Liu and S.-J. Bao, *Microchim. Acta*, 2018, **185**, 140.

34 R. Doufnoune and N. Haddaoui, *J. Polym. Res.*, 2017, **24**, 138.

35 K. Liu, L. Chen, Y. Chen, J. Wu, W. Zhang, F. Chen and Q. Fu, *J. Mater. Chem.*, 2011, **21**, 8612–8617.

36 S. Thakur and N. Karak, *Carbon*, 2012, **50**, 5331–5339.

37 H.-C. Liu, W.-H. Ho, C.-F. Li and S.-K. Yen, *J. Electrochem. Soc.*, 2008, **155**, E178–E182.